

Shear Behavior and Mode of Failure for ASTM C1433 Precast Box Culverts

Ali Abolmaali¹ and Anil Garg²

Abstract: This study evaluates the shear behavior and capacity of the precast concrete box culverts subjected to HS 20 truck wheel load. The most critical culvert behavior was considered by studying culverts subjected to zero depth of the fill and placed on a rigid bedding material. Full-scale experimental tests, with wheel load placed at the distance d from the tip of the haunch to the edge of the load plate, were conducted on 24 typical precast concrete box culverts designated as per ASTM C1433-05. The test results further indicated that flexure governed the behavior up to and beyond AASHTO 2005 factored load. Three-dimensional nonlinear finite-element models (FEMs) of the test specimens were developed and verified with the experimental results. The three-dimensional volumetric shear force distributions on the top slab of the 42 ASTM C1433-05 boxes were obtained by using the FEM from which the distribution width for each box was calculated. This was used to obtain the critical factored shear force for all the boxes which were then compared with the American Concrete Institute shear capacity equations. It was shown that the shear capacity exceeded the factored critical shear force for all the ASTM C1433-05 boxes. This study shows that the AASHTO 2005 provision with regard to the shear transfer device across the joint is unsupported.

DOI: 10.1061/(ASCE)1084-0702(2008)13:4(331)

CE Database subject headings: Failure modes; Culverts; Concrete, precast; Bridges, highway; Shear.

Introduction

The shear behavior of precast box culverts with less than 0.61 m (2 ft) has been somehow a controversial issue with different viewpoints. The AASHTO (2005) specifications state that shear transfer device should be provided across the joint, if the calculated distribution width exceeds the length between the two adjacent joints. Prior to the AASHTO (2005) specifications (AASHTO 1998; AASHTO 2002), culverts were not required to be designed with joints for direct shear transfer. This was based on the research studies conducted by James (1984) and Frederick et al. (1988), which reported that shear transfer was not critical with zero fill depth across the joint due to the small deflections and strains that caused no cracks at service load. However, both the aforementioned studies placed the wheel live load at the edge of the bell or spigot ends at the middle of the culvert's span during their experimental testing and/or modeling. Therefore, this raised concerns that the wheel load location may not have produced the critical shear stresses since it was placed away from the vicinity of the culvert's wall (support).

¹Associate Professor, Dept. of Civil and Environmental Engineering, Professor-in-Charge, Structural Simulation Laboratory, Director, UT Arlington Center for Structural Engineering Research, The Univ. of Texas at Arlington, Arlington, TX 76019 (corresponding author). E-mail: abolmaali@uta.edu

²Postdoctoral Fellow, Dept. of Civil and Environmental Engineering, Structural Simulation Laboratory, The Univ. of Texas at Arlington, Arlington, TX 76019. E-mail: agarg.us@gmail.com

Note. Discussion open until December 1, 2008. Separate discussions must be submitted for individual papers. To extend the closing date by one month, a written request must be filed with the ASCE Managing Editor. The manuscript for this paper was submitted for review and possible publication on October 30, 2006; approved on November 7, 2007. This paper is part of the *Journal of Bridge Engineering*, Vol. 13, No. 4, July 1, 2008. ©ASCE, ISSN 1084-0702/2008/4-331-338/\$25.00.

To identify the effect of the wheel load location, McGrath AASHTO et al. (2004) used the finite-element method (FEM) to investigate the live load distribution widths for reinforced concrete box culverts by placing the wheel live load at a distance d (=effective depth of top slab) from the tip of the haunch to the edge of the load plate. Two-dimensional shell elements were used to conduct linear elastic analyses of several parametric cases. This study concluded that the distribution width for shear in general was narrower than that of positive and negative bending moments, and it governed the design. The results of this study are implemented in AASHTO (2005) with new distribution width equations based on shear force distribution, and it was suggested that a shear transfer device should be provided across the joint, if the calculated distribution width exceeds the length between the two adjacent joints.

Since the FEM analyses conducted by McGrath et al. (2004) were linear elastic without experimental verification, this study was undertaken. This paper reports on the findings of a comprehensive full-scale experimental and analytical study to identify the shear strength and behavior of the ASTM C1433-05 box culverts. Twenty four culverts were designed per ASTM C1433-05, and they were tested by placing the load at the distance d from the tip of the haunch to the edge of the load plate, which were manufactured by Hanson Pipe and Products and Rinker Hydro Conduit in the United States. Complete nonlinear three-dimensional FEMs of the boxes were developed from which all the ASTM C1433-05 boxes were analyzed. The distribution width and the critical factored shear forces were calculated and compared with the American Concrete Institute (ACI) strength equations.

Test Cases

Twenty four cases were selected for various spans and joint lengths. Spans of 91 cm (3 ft), 122 cm (4 ft), 244 cm (8 ft), and

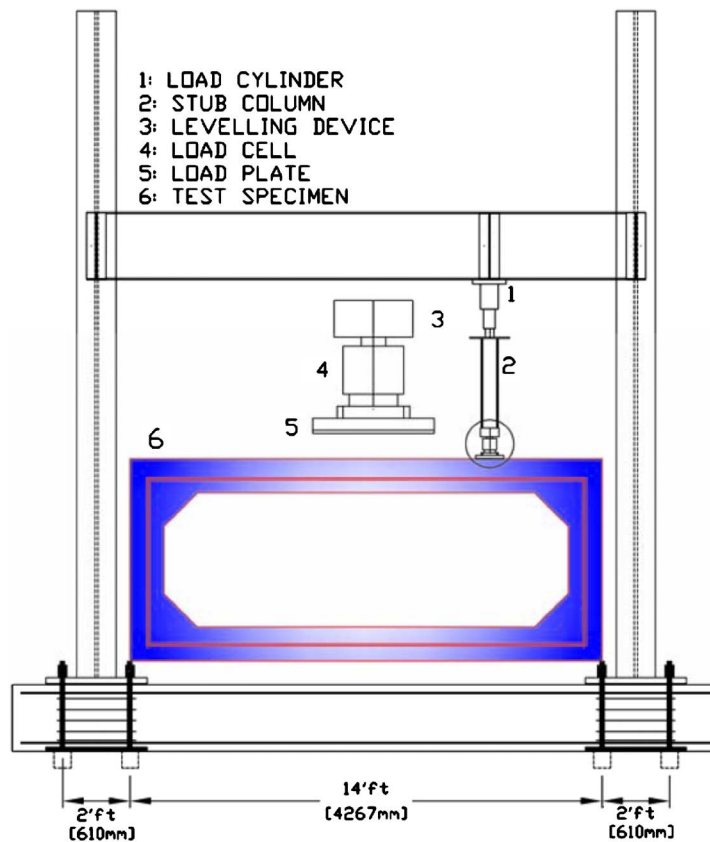


Fig. 1. Typical test setup and instrumentation

366 cm (12 ft) were tested with a joint length of 122 cm (4 ft) for all the spans tested and 244 cm (8 ft) for the spans of 122 cm (4 ft) and 244 cm (8 ft).

Depending upon the span length, the thickness of the top slab varied from 17.8 cm (7 in.) to 30.5 cm (12 in.), bottom slab's thickness varied from 15.2 cm (6 in.) to 30.5 cm (12 in.), and wall's thickness varied from 12.7 cm (5 in.) to 30.5 cm (12 in.). The haunches' dimensions also varied from 12.7 (5 in.) to 30.5 cm (12 in.).

The reinforcement cages consisted of plain welded wires as per ASTM A 185 (ASTM 2001). The size of the steel wires used for the reinforcement cages ranged from W2.0 to W8.0 with their areas varying from 12.90 mm² (0.02 in.²) through 51.61 mm² (0.08 in.²) per reinforced wire. The nominal diameter of each wire ranged from 4 to 8 mm (0.159–0.319 in.). Typical spacing of wires was 5 cm (2 in.), 10 cm (4 in.), and 15 cm (6 in.).

Different loading positions were tested to examine the behavior of each box culvert. Tests were conducted on the spigot end or the bell end of each culvert. The box was either with or without compression distribution steel in the top slab known as A_{S6} . The following nomenclature was used to identify each test specimen SP or BL_S-R-L_N or Y_lx where SP=spigot end; BL=bell end; S-R-L=dimension of the culvert [cm (ft)] (span of the top slab, rise, and the joint length); N=no distribution reinforcement (A_{S6}); Y=with distribution reinforcement (A_{S6}); lx=distance between the tip of the haunch to the edge of the load plate in terms of d .

Test Setup

The Engineering Lab Building, University of Texas, Arlington (ELB) test setup consisted of a reaction frame with four W12

× 87 steel columns welded to 90 cm × 90 cm (35 1/2 in. × 35 1/2 in.) base plates with a thickness of 5.1 cm (2 in.), (Fig. 1).

A 25 cm × 51 cm × 2.54 cm (10 in. × 20 in. × 1 in.) mild steel load plate supported by a 1.27 cm (1/2 in.) thick rubber sheet was placed on the top of the box culvert as shown in Fig. 1. This was done to simulate the contact area of the wheel of a HS20 truck or tandem, having an axle load of 142 kN (32 kip) and wheel load of 71 kN (16 kip). A 890 kN (200 kip) capacity precalibrated load cell was placed on the top of the load plate. Each test box culvert was placed directly on the top of the reaction floor to produce the maximum stress state in the culvert which would yield to the most critical condition. A laser-based optoelectronic displacement sensor in addition to a displacement transducer was used to accurately measure the deflection under the load plate in two different ways. An incremental loading history was applied in order to accurately capture the nonlinear load deflection behavior (Abolmaali and Garg 2008; Garg 2007).

Finite-Element Modeling

Nonlinear three-dimensional (3D) FEM of the test condition was developed by using ABAQUS 6.6 software (ABAQUS 2006), the results of which were compared with the three experimental tests (Fig. 2). The models included (3D) solid (C3D8R) and 3D shell (SC8R) elements having geometric and material nonlinearities. The reinforcement was modeled by rebar elements which were placed on three-dimensional four-noded surface element (SFM3D4). The base support (strong reaction floor) was also modeled by modeling a rectangular block with a high stiffness

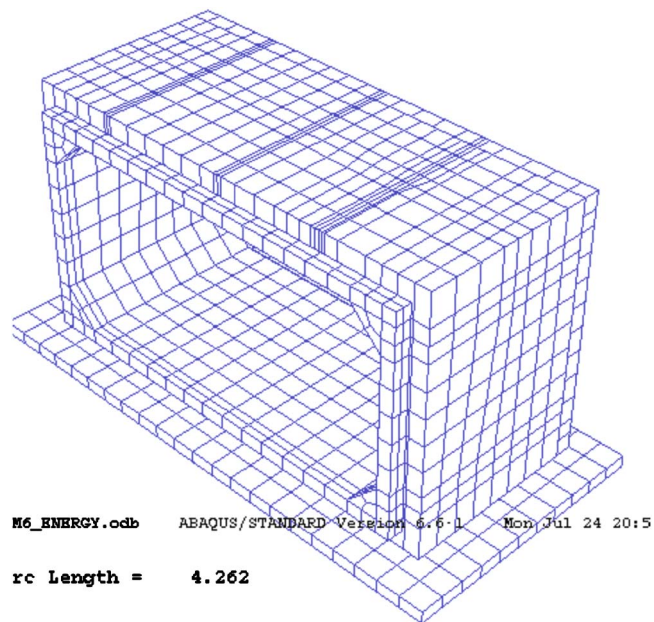


Fig. 2. Typical FEM mesh

value. The contact between the box and the reaction floor was modeled by using node-to-surface contact elements. The boxes were loaded on an area equal to the wheel load plate 30 cm \times 51 cm (10 in. \times 20 in.). The incremental wheel load was applied using Riks method (Crisfield 1986) up to 445 kN (100 kip), the approximate load at which most of the test specimens failed during the experimental testing. The cracking strains were studied for all the load steps for all the boxes tested using brick (C3D8R) elements. The amount of plastic strain needed to reduce the stresses to zero at crack, known as tension stiffening (Biggs et al. 2000) was used in controlling the stiffness of the model. The tension stiffening parameter was determined and compared with those reported by Torres et al. (2004). The smeared crack model algorithm was adopted as introduced by Kwak and Filippou (1990). The elements cracking strain at specified load levels were identified. The energy convergence approach was adopted due to the nonlinear nature of the problem, and the fact that monotonic converges of nonlinear problems based on mesh density refinement (H -convergence) alone are not guaranteed (Razavi 2004 and Razavi et al. 2006).

Experimental and FEM Results

The full-scale experimental tests indicated that flexure governed the behavior for all the test specimens up to and beyond the AASHTO (2005) factor live load. For all the test specimens, the flexural cracks formed initially on the inside face of the top or bottom slab, which extended to the spigot or bell toward the middle of the load plate. No flexural cracks were observed at loads below the AASHTO (2005) service load.

The second series of cracks, for all the test specimens, were negative moment cracks which formed on the wall closest to the load plate along the joint length at a distance equal to approximately one third from the top slab. These cracks normally extended to the spigot and bell ends.

The third series of cracks were noticed to be the negative moment cracks which initiated at both walls and extended to the outside face of the top slab. In some tests, these cracks extended

along the span on the outside face of the top slab.

The shear cracks were among the final cracks observed. For all of the test specimens, shear cracks formed at approximately 320 kN (72 kip) of load (almost twice the AASHTO factored load). These cracks initiated independently from the tip of the haunch (on the testing end [spigot or bell]) and extended toward the edge of the load plate. By independent shear crack, we mean that it did not initiate at the tip of the flexural cracks. No shear crack was observed before flexural cracks in any of the specimens tested.

A comparison of the FEM and the experimental results for crack initiation and propagation of cracks showed close correlation. The crack predictions by the FEM analyses were similar to those observed in the experiments for the particular load level and crack location. The comparison of the crack pattern of a typical test specimen with the FEM results is presented in Fig. 3. In general, the FEM predicted the crack patterns closely for all the test specimens.

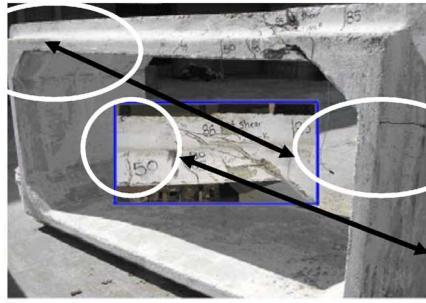
The typical load deflection plots obtained from the experiments are compared with those obtained from FEM analyses and are presented in Figs. 4 and 5 for 244 cm (8 ft) and 366 cm (12 ft) span culverts, respectively. In these figures, the experimental load deflection plots are presented for the AASHTO (2005) factored load. Fig. 5 shows the experimental results for tests with and without top slab distribution steel (A_{s6}). As shown, the effect of A_{s6} is negligible and this comparison was consistent for all the test specimens. A comprehensive FEM verification for all the test specimens is presented by Abolmaali and Garg (2008), Garg and Abolmaali (2008), and Garg (2007).

Shear Capacity of ASTM C1433

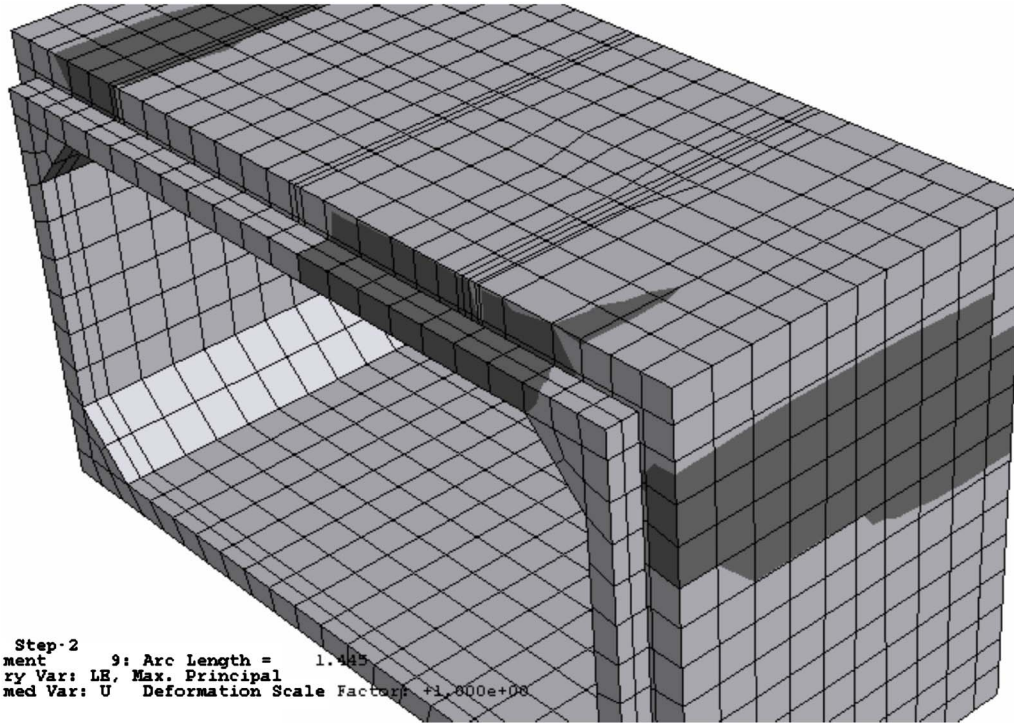
Distribution width is a concept used in the design of slabs in which the strength of a specified width is required to resist the bending moment developed due to any standard loading. This is commonly adopted by the AASHTO specifications for designing the bridge decks. In AASHTO (2005) the same concept is utilized based on the McGrath et al. (2004) study to conclude that since shear distribution width was reported to be small, a shear transfer device was required across the joint of the connected culverts. Since the experimental testing program of this study indicated that the shear behavior was not the governing factor in any of the box culverts tested until the loads up to at least twice the factored design load, it led the investigators to believe that the relationship between the magnitude of the distribution width and the actual box behavior, as presented in AASHTO (2005) is misleading. Thus, the distribution width for all the boxes of ASTM 1433 was calculated and compared with the ACI shear strength equations.

To calculate the shear distribution width, the volumetric shear force distribution for the top slab is plotted as shown in Fig. 6(a), and a vertical plane is passed through the location at which the shear force is maximum along the joint length. To obtain the distribution width, the area under the shear force diagram obtained from this vertical cut is calculated and then divided by the value of maximum shear force. This basically means that by multiplying the distribution width with the peak shear force, an equivalent rectangular area representing the area under the 2D shear force distribution is obtained [Fig. 6(b)].

The values of distribution width for the ASTM C1433 boxes calculated in this study are based on the factored wheel load, which are less than those calculated per AASHTO (2005). Indeed, the AASHTO distribution width for each box of C 1433 is at least



Experimental Cracks



FEM Cracks

Fig. 3. Experimental versus FEM cracks

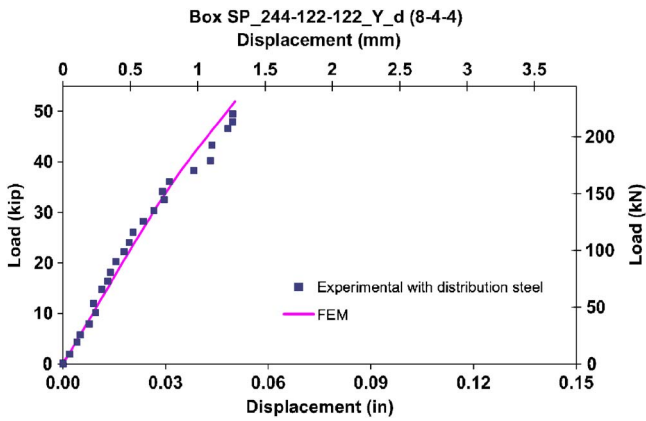


Fig. 4. Comparison of FEM with experimental data for SP_244-122-122_Y_d(SP_8-4-4_Y_d)

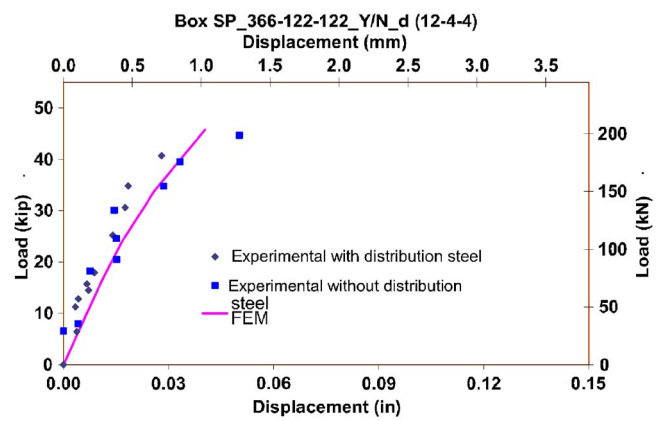


Fig. 5. Comparison of FEM with experimental data for SP_366-122-122_Y/N_d(SP_12-4-4_Y/N_d)

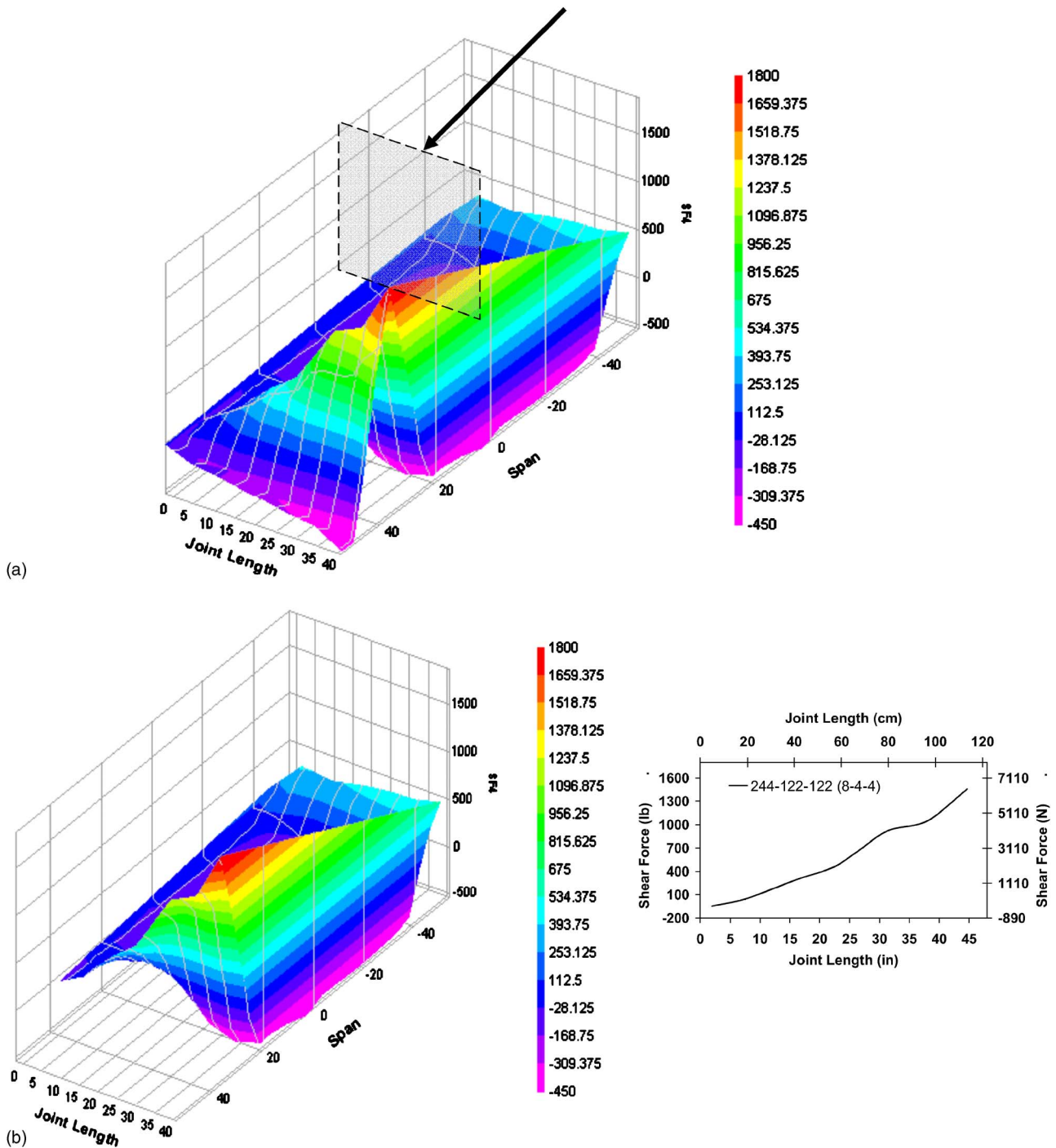


Fig. 6. Typical volumetric shear force plot showing cutting plane at point of maximum shear force: (a) typical volumetric shear force plot showing cutting plane at point of maximum shear force; (b) shear force plot in volume and in area at point of maximum shear force

three to four times those calculated based on the FEM in this study (Abolmaali and Garg 2008, Garg and Abolmaali 2006, and Garg et al. 2006). Furthermore, the distribution width values were used to calculate the critical factored shear force values as presented in column 3 of Table 1, which was compared with the two ACI shear capacity equations: $2b_w d \sqrt{f'_c}$ (referred from this point forward as lower bound shear strength equation) and $3.5b_w d \sqrt{f'_c}$ (referred from this point forward as upper bound shear strength equation). It should be noted that the former is used for scenarios in which shear cracks form at the tip of existing flexural cracks while the latter is used for cases in which shear cracks initiates at

a 45° angle independent of flexural cracks. All the experimental testing conducted by Abolmaali and Garg (2008) and Garg (2007) indicated that the shear cracks initiated independently at the tip of the haunch at approximately twice the factor loads with nearly 45° angles. This indicates that the $3.5b_w d \sqrt{f'_c}$ = applicable shear strength equation for the precast box culverts.

Referring back to Table 1, the ratio between the aforementioned lower and upper bound strength equations and the critical factored shear force is calculated and presented in columns 5 and 6, respectively. Column 5 shows that the range of these ratios varies from 0.64 to 1.04 with 60% of them between 0.90 and

Table 1. Shear Strength versus Shear Load on Box Culvert at Factored Load per AASHTO (2005)

Span-rise-length_with/without dist. steel_ I_w [cm (ft)]	Factored critical shear V_c [cm kN/cm (in. kip/in.)]	Shear strength [kN (kip)] applicable SI unit strength equation		Shear strength/ shear force	
		$2b_w d \sqrt{f'_c}$	$3.5b_w d \sqrt{f'_c}$	$2b_w d \sqrt{f'_c} / V_c$	$3.5b_w d \sqrt{f'_c} / V_c$
SP_366-366-122_N_d	133	133	237	1.02	1.78
(SP_12-12-4_N_d)	(30.00)	(30.00)	(53.34)		
SP_366-305-122_N_d	133	133	238	1.02	1.79
(SP_12-10-4_N_d)	(29.93)	(29.93)	(53.56)		
SP_366-244-122_N_d	133	133	240	1.03	1.80
(SP_12-8-4_N_d)	(30.00)	(30.00)	(53.89)		
SP_366-183-122_N_d	135	135	243	1.02	1.79
(SP_12-6-4_N_d)	(30.44)	(30.44)	(54.53)		
SP_366-122-122_N_d	136	136	247	1.04	1.82
(SP_12-4-4_N_d)	(30.53)	(30.53)	(55.50)		
SP_335-335-122_N_d	131	131	210	0.92	1.61
(SP_11-11-4_N_d)	(29.46)	(29.46)	(47.32)		
SP_335-305-122_N_d	131	131	211	0.92	1.61
(SP_11-10-4_N_d)	(29.51)	(29.51)	(47.47)		
SP_335-244-122_N_d	130	130	212	0.93	1.63
(SP_11-8-4_N_d)	(29.30)	(29.30)	(47.73)		
SP_335-183-122_N_d	133	133	215	0.93	1.62
(SP_11-6-4_N_d)	(29.80)	(29.80)	(48.27)		
SP_335-122-122_N_d	134	134	217	0.93	1.62
(SP_11-4-4_N_d)	(30.09)	(30.09)	(48.89)		
SP_305-305-122_N_d	128	111	194	0.86	1.51
(SP_10-10-4_N_d)	(28.88)	(24.93)	(43.63)		
SP_305-274-122_N_d	129	111	195	0.86	1.51
(SP_10-9-4_N_d)	(28.96)	(25.00)	(43.75)		
SP_305-244-122_N_d	129	112	195	0.86	1.51
(SP_10-8-4_N_d)	(29.06)	(25.07)	(43.87)		
SP_305-213-122_N_d	130	112	197	0.86	1.51
(SP_10-7-4_N_d)	(29.21)	(25.25)	(44.19)		
SP_305-183-122_N_d	130	112	196	0.86	1.51
(SP_10-6-4_N_d)	(29.28)	(25.23)	(44.16)		
SP_305-152-122_N_d	131	113	197	0.86	1.51
(SP_10-5-4_N_d)	(29.44)	(25.35)	(44.37)		
SP_274-274-122_N_d	126	94	165	0.75	1.31
(SP_9-9-4_N_d)	(28.38)	(21.23)	(37.15)		
SP_274-244-122_N_d	127	94	165	0.75	1.31
(SP_9-8-4_N_d)	(28.44)	(21.22)	(37.13)		
SP_274-213-122_N_d	127	95	166	0.75	1.31
(SP_9-7-4_N_d)	(28.49)	(21.30)	(37.28)		
SP_274-183-122_N_d	127	95	166	0.75	1.31
(SP_9-6-4_N_d)	(28.55)	(21.30)	(37.28)		
SP_274-152-122_N_d	128	95	167	0.75	1.31
(SP_9-5-4_N_d)	(28.67)	(21.41)	(37.47)		
SP_244-244-122_N_d	121	83	145	0.68	1.20
(SP_8-8-4_N_d)	(27.15)	(18.59)	(32.52)		
SP_244-213-122_N_d	121	83	145	0.68	1.20
(SP_8-7-4_N_d)	(27.25)	(18.63)	(32.60)		
SP_244-183-122_N_d	122	83	145	0.68	1.20
(SP_8-6-4_N_d)	(27.35)	(18.69)	(32.71)		
SP_244-152-122_N_d	122	83	146	0.68	1.19
(SP_8-5-4_N_d)	(27.46)	(18.73)	(32.78)		
SP_244-122-122_N_d	123	84	146	0.68	1.19
(SP_8-4-4_N_d)	(27.60)	(18.78)	(32.86)		

Table 1. (Continued.)

Span-rise-length_with/without dist. steel I_w [cm (ft)]	Factored critical shear V_c [cm kN/cm (in. kip/in.)]	Shear strength [kN (kip)] applicable SI unit strength equation		Shear strength/shear force	
		$2b_w d \sqrt{f'_c}$	$3.5b_w d \sqrt{f'_c}$	$2b_w d \sqrt{f'_c} / V_c$	$3.5b_w d \sqrt{f'_c} / V_c$
SP_213-213-122_N_d (SP_7-7-4_N_d)	124 (27.79)	79 (17.70)	138 (30.97)	0.64	1.11
SP_213-183-122_N_d (7-6-4_N_d)	124 (27.88)	79 (17.78)	138 (31.11)	0.64	1.12
SP_213-152-122_N_d (SP_7-5-4_N_d)	124 (27.97)	79 (17.82)	139 (31.18)	0.64	1.11
SP_213-122-122_N_d (SP_7-4-4_N_d)	125 (28.12)	80 (17.90)	139 (31.33)	0.64	1.11
SP_183-183-122_N_d (SP_6-6-4_N_d)	118 (26.60)	79 (17.86)	139 (31.25)	0.67	1.17
SP_183-152-122_N_d (SP_6-5-4_N_d)	119 (26.68)	80 (17.90)	139 (31.32)	0.67	1.17
SP_183-122-122_N_d (SP_6-4-4_N_d)	119 (26.80)	80 (18.00)	140 (31.50)	0.67	1.18
SP_183-91-122_N_d (SP_6-3-4_N_d)	120 (26.96)	80 (18.06)	141 (31.60)	0.67	1.17
SP_152-152-122_N_d (SP_5-5-4_N_d)	112 (25.23)	80 (18.01)	140 (31.52)	0.71	1.25
SP_152-122-122_N_d (SP_5-4-4_N_d)	113 (25.29)	80 (18.04)	140 (31.58)	0.71	1.25
SP_152-91-122_N_d (SP_5-3-4_N_d)	113 (25.46)	81 (18.31)	143 (32.05)	0.72	1.26
SP_122-122-122_N_d (SP_4-4-4_N_d)	60 (13.52)	62 (14.04)	109 (24.56)	1.04	1.82
SP_122-91-122_N_d (SP_4-3-4_N_d)	59 (13.35)	63 (14.25)	111 (24.94)	1.07	1.87
SP_122-61-122_N_d (SP_4-2-4_N_d)	58 (13.02)	63 (14.26)	111 (24.95)	1.09	1.92
SP_91-91-122_N_d (SP_3-3-4_N_d)	61 (13.81)	56 (12.64)	98 (22.13)	0.92	1.60
SP_91-61-122_N_d (SP_3-2-4_N_d)	59 (13.32)	56 (12.55)	98 (21.96)	0.94	1.65

1.04, and the remaining 40% falls between 0.64 and 0.90. Column 6 shows that 100% of the calculated ratios are above 1.0 with their range varying from 1.10 to 1.80 from which over 50% of the ratios are above 1.50. Thus, it is shown that the shear strength of the ASTM C1433 box culverts is more than adequate with the upper bound shear (applicable) strength equation. When comparing with the lower bound shear strength equation, 60% of the ASTM C1433 boxes are considered adequate.

It should be noted that the lower bound shear strength equation is not applicable to the precast box culverts based on the experimental observations, and it is only presented here for comparison purposes. However, since this study was conducted based on the culverts subjected to the most critical stresses (no bedding materials and zero depth of the fill), it is anticipated that for the less severe loading condition when bedding material, depth of fill, and lateral soil are accounted for, the majority of the boxes will satisfy the lower bound shear strength equation as well.

Table 1 also shows that the minimum calculated ratios of strength to critical shear force are obtained for the 183 cm (6 ft), 213 cm (7 ft), and 244 cm (8 ft) span box culverts. This is due to

the fact that there is negligible difference between the peak shear force for boxes with spans 183 cm (6 ft), 213 cm (7 ft), 244 cm (8 ft), 274 cm (9 ft), 305 cm (10 ft), 335 cm (11 ft), and 366 cm (12 ft) (Garg et al. 2006) while the top slab thickness for the 183 cm (6 ft), 213 cm (7 ft), and 244 cm (8 ft) span boxes are 18 cm (7 in.), 20 cm (8 in.), 20 cm (8 in.), respectively, which are considerably less than the values of slab thickness for 23 cm (9 in.), 25 cm (10 in.), 28 cm (11 in.), and 30 cm (12 in.) for the 274 cm (9 ft), 305 cm (10 ft), 335 cm (11 ft), and 366 cm (12 ft) span boxes, respectively.

The above observations further contradicted the relationship between the distribution width and shear capacity presented in AASHTO (2005) which was based on the study conducted by McGrath et al. (2004). While distribution width values calculated in this study were less than those calculated based on AASHTO 2005, it was shown that the shear capacity of the ASTM C1433 boxes were more than adequate. Since this conclusion is drawn based on the experimental observation and FEM studies conducted in this research, it is concluded that the distribution width equations presented in AASHTO (2005) for the box culverts does

not represent the true culvert behavior. This statement is particularly supported since the study presented by McGrath et al. (2004) was based on 2D linear elastic finite-element analyses on 3D geometry, which was neither supported nor validated by experimental observations. Moreover, since linear elastic analyses were conducted, they were unable to establish a relationship between the distribution width and the box culvert failure mode. Thus, they compared the distribution width for shear to the distribution width for bending moment, and they concluded that the lesser distribution width controls the failure mechanism.

This study disputes the McGrath et al. (2004) findings and argues that the governing mode of failure is flexure rather than shear even though the wheel load is placed at the distance d from the tip of the haunch. This behavior was observed during the extensive experimental testing and analytical investigations (Abolmaali and Garg 2008). Furthermore, the culvert's behavior unlike the traditional bridge slab is governed by the additional joint rotation induced during loading, which will introduce additional bending moment in the culvert's top slab and cause the flexural cracks to govern the behavior up to and beyond the AASHTO factored wheel load.

The writers acknowledge that AASHTO specifications apply to culverts other than ASTM C1433 (ASTM 2003) such as those with thin slab thickness for special type designs. However, all the values of the slab thickness used in the McGrath et al. (2004) study were based on slab thicknesses similar to ASTM C1433 boxes, which forces the writers to insist on the shortcomings of AASHTO (2005) with respect to governing distribution width based on shear.

Conclusion

All the 42 standard cases of the ASTM C 1433 (ASTM 2003) were modeled using the experimentally verified FEM. The FEM model analyses were used to plot the 3D volumetric shear force distribution on the top slab of the boxes analyzed. The peak shear force in each of the plots was identified and a vertical plane, parallel to the box's joint length, was passed through it. This yielded to a 2D shear force distribution diagram along the box joint length from which the distribution width was calculated.

The calculated values of the distribution width were used to evaluate the critical factored shear force for all the boxes of ASTM C 1433 and were then compared with the American Concrete Institute (ACI) shear capacity equations. It was shown that the shear capacity exceeded the factored critical shear force for all the ASTM C1433 boxes.

This study concludes that the AASHTO provisions for box culverts, obtained from the McGrath et al. (2004) study based on their linear elastic finite-element analysis, is incapable of predicting culverts' behavior, and it needs to be revisited.

Furthermore, the AASHTO (2005) provisions, which state "shear transfer device should be provided across the joint, if the calculated distribution width exceeds the length between the two adjacent joints" is unsupported.

Acknowledgments

The financial support of the National Science Foundation, Federal Highway Institute, and the American Concrete Pipe Association are gratefully acknowledged. The assistance of Dr. Raul Fernan-

dez from the Automation Robotic Research Institute in providing expertise with laser instrumentation is highly appreciated.

References

- AASHTO. (1998). *AASHTO LRFD bridge design specifications*, 2nd Ed., Washington, D.C.
- AASHTO. (2002). *AASHTO standard specifications for highway bridges*, 17th Ed., Washington, D.C.
- AASHTO. (2005). *Interim AASHTO LRFD bridge design specifications*, 3rd Ed., Washington, D.C., 3.14, 12.80.
- ABAQUS. (2006). *ABAQUS manual* Version 6.6, Pawtucket, R.I.
- Abolmaali, A., and Garg, A. K. (2008). "Effect of wheel live load on shear behavior of precast reinforced concrete box culverts." *J. Bridge Eng.*, 13(1), 93–99.
- ASTM. (2001). "Standard specification for steel welded wire reinforcement, plain, for concrete." *A185*, West Conshohocken, Pa.
- ASTM. (2003). "Standard specification for precast reinforced concrete box sections for culverts, storm drains, and sewers." *C1433-03*, West Conshohocken, Pa.
- Biggs, R. M., Barton, F. W., Gomez, J. P., Massarelli, P. J., and McKeel, W. T., Jr. (2000). "Finite-element modeling and analysis of reinforced-concrete bridge decks." *VTRC 01-R4*, Virginia Transportation Research Council, Federal Highway Administration, Washington D.C., 1–23.
- Crisfield, M. A., (1986). "Snap-through and snap-back response in concrete structures and the dangers of under-integration." *Int. J. Numer. Methods Eng.*, 22, 751–767.
- Federick, G. R., Ardis, C. V., Tarhini, K. M., and Koo, B., (1988). "Investigation of the structural adequacy of C 850 box culverts." *Transportation Research Record. 1191*, Transportation Research Board, Washington D.C., 73–80.
- Garg, A. K. (2007). "Experimental and finite-element based investigation of shear behavior in reinforced concrete box culverts." Ph.D. dissertation, Univ. of Texas at Arlington, Arlington, Tex.
- Garg, A. K., and Abolmaali, A. (2006). "Shear behavior of small span single and double precast reinforced concrete box culverts." *Proc. of the ASCE Pipeline Division Specialty Conf. Pipelines 2006 Service to the Owner* (CD ROM), Chicago.
- Garg, A. K., and Abolmaali, A. (2008). "Finite-element modeling and analysis of reinforced concrete box culverts." *J. Transp. Eng.*, in press.
- Garg, A. K., Abolmaali, A., and Fernandez, R. (2006). "Experimental investigation of shear capacity of precast reinforced concrete box culverts." *J. Bridge Eng.*, 12(4), 511–517.
- James, R. W. (1984). "Behavior of ASTM C 850 concrete box culverts without shear connectors." *Transportation Research Record. 1001*, Transportation Research Board, Washington, D.C., 104–111.
- Kwak, H. G., and Filippou, F. C. (1990). *Finite-element analysis of reinforced concrete structures under monotonic loads*, Structural Engineering, Mechanics and Materials, Department of Civil Engineering, University of California Press, Berkeley, Calif.
- McGrath, T. J., Liepins, A. A., Beaver, J. L., and Strohmman, B. P. (2004). "Live load distribution widths for reinforced concrete box culverts." *A study for the Pennsylvania Department of Transportation*, Simpson Gumpertz & Heger Inc., Boston.
- Razavi, H. (2004). "Kinematic hardening cyclic plasticity-based semi-meshless finite-element algorithm for contact and bolted problems in computational mechanics." Ph.D. dissertation, Univ. of Texas at Arlington, Arlington, Tex.
- Razavi, H., Abolmaali, A., and Ghassemieh, M. (2006). "Invisible elastic bolt model concept for finite-element analysis of bolted connections." *J. Constr. Steel Res.*, in press.
- Torres, L., Lopez-Almansa, F., and Bozzo, L. M., (2004). "Tension-stiffening model for cracked flexural concrete members." *J. Struct. Eng.*, 130(8), 1242–1251.